Journal of Solid State Chemistry 181 (2008) 2796–2803

Contents lists available at ScienceDirect

Journal of Solid State Chemistry

journal homepage: www.elsevier.com/locate/jssc

One-step catalyst-free generation of carbon nanospheres via laser-induced pyrolysis of anthracene

M. Bystrzejewski [a,c,*], H. Lange [a], A. Huczko [a], P. Baranowski [a], H.-W. Hübers [b], T. Gemming [c], T. Pichler [c], B. Büchner [c], M.H. Rümmeli [c]

[a] Department of Chemistry, Warsaw University, Pasteur 1 Str., 02-093 Warsaw, Poland
[b] German Aerospace Centre (DLR), Rutherfordstr.2, D-12489 Berlin, Germany
[c] IFW Dresden, Helmoltzstr. 20, 01069 Dresden, Germany

ARTICLE INFO

Article history:
Received 29 January 2008
Received in revised form
7 July 2008
Accepted 9 July 2008
Available online 20 July 2008

Keywords:
Carbon nanoparticles
Laser pyrolysis
Raman spectroscopy
Electron microscopy

ABSTRACT

Carbon nanospheres with diameters between 100 and 400 nm have been successfully synthesized via low-power laser-assisted pyrolysis of anthracene in a nitrogen atmosphere. The developed facile route yields homogeneous nanoparticles and requires no supplementary carbon feedstock or catalyst. The sharp thermal gradient afforded by the laser results in two kinds of carbon products that differ in crystallinity and mean particle size. Our detailed findings point to the carbon nanospheres being comprised of small-unclosed aromatic layers that are connected together by simple organic linkers. C–H bonds in the anthracene molecules are partially broken by the laser beam energy, and as the newly created large radicals aggregate, carbon nanospheres are formed.

1. Introduction

Carbon's ability to hybridize as *sp*, sp^2 and sp^3 bonds results in the formation of a variety of structures, such as fullerenes [1], nanotubes and nanofibers [2], nanoonions [3], nanocapsules [4], and carbon nanospheres (CNS) [5–7].

In comparison to the level of studies on fullerenes, nanotubes or nanofibers, the reports on CNS are relatively few. Nonetheless CNS are of considerable interest due to their intrinsic chemical and physical properties. CNS are different to fullerenes or carbon nanoonions, because they have unclosed graphene-like layers. The semi-crystalline structure of CNS is reflected in their unique properties: (i) low density, (ii) high porosity and surface area, and (iii) relatively high chemical and thermal stability [8]. CNS have many prospective applications, e.g. as catalysts supports [9], lubricating agents [10], electrode materials [11,12], and in the construction of advanced sensors [13,14]. Further, recent studies have shown that CNS provide efficient storage of ethylene [15].

A variety of routes have been developed to synthesize CNS: chemical vapor deposition (CVD) [16–18], pyrolysis of hydrocarbons [5,8], decomposition of polymers [19,20], high-pressure-induced reactions [6,21–23] or hydrothermal synthesis [7]. CNS have even been synthesized via the sonication of pyrolytic graphite [24]. CNS have also been obtained by using more sophisticated experimental systems, e.g. RF plasma enhanced CVD or low-pressure deposition of gaseous carbon at 2800–2900 K [25]. By far, most of these methods require a catalyst, which results in unwanted by-products. This requires purification making the process more complicated and costly. Thus, there is a pressing need for the production of CNS via a *catalyst-free* system. Moreover, the use of low cost and environmentally friendly starting materials, and a facile production route are obviously attractive.

Laser-based methods have been widely used in the synthesis of various nanocarbon materials, including nanotubes [26–29]. Recently, a novel laser-assisted route for the synthesis of carbon nanotubes was shown. The technique was based on the decomposition of organo-metallic compounds with a relatively low-power continuous wave (CW) CO_2 laser beam [30]. The synthesis occurs at much lower temperatures than with standard laser ablation techniques.

In addition, high-energy pulsed laser pyrolysis of aliphatic and aromatic hydrocarbons only yields amorphous carbon nanoparticles and a variety of gaseous products [31–33]. CO_2 laser pyrolysis of benzene catalyzed with $Fe(CO)_5$ resulted in carbon nanoparticles and nanonions along with a few fullerenes, which were predominantly C_{60} [32]. In this contribution we detail a synthesis route, which fulfils all of the above-discussed criteria for catalyst-free CNS synthesis. In this newly developed route, a

* Corresponding author at: Department of Chemistry, Warsaw University, Pasteur 1 Str., 02-093 Warsaw, Poland. Fax: +48 22 822 59 96.
E-mail address: mibys@chem.uw.edu.pl (M. Bystrzejewski).

0022-4596/$ - see front matter © 2008 Elsevier Inc. All rights reserved.
doi:10.1016/j.jssc.2008.07.012

relatively low-power continuous CO_2 laser beam is used to decompose anthracene in an N_2 atmosphere. Moreover, no catalyst or supplementary hydrocarbon is required. The developed novel and facile laser-induced pyrolysis route yields homogeneous CNS. The resultant CNS have been characterized in detail using a broad variety of techniques.

2. Experimental

The experimental set-up is illustrated in Fig. 1 (left panel). It consists of a KF40 glass four-cross. On one port a ZnSe window is attached. On the opposite port a purpose built adjustable target holder is mounted. The other two ports provide adjustable gas entry and exit ports. In these studies, N_2 was used as the gas throughout with a flow rate of 0.4 l/min and pressure of 1 bar. The targets were pressed in a 13 mm die and were typically 3 mm thick. The target consisted of a mix of anthracene with pure graphite (powder weight ratio = 7:3). The addition of graphite to the matrix improves the laser coupling to the target and the heat exchange between the anthracene crystallites to enable the reaction to occur. Prior to the reaction, the chamber was thoroughly flushed with N_2, after which the flow rate was lowered (0.4 l/min) and the laser was then fired onto the target. The laser spot size is about 3 mm. The CO_2 continuous laser power was maintained at 30 W. The temperature on the spot was between 1000 and 1300 K. This is sufficient to decompose the anthracene while not evaporating the graphite. The reaction times used varied between 30 and 90 s. The sharp thermal gradient on the target from the laser irradiation resulted in two reaction zones: (i) pyrolysis zone (its size being dictated by the laser beam spot size) and (ii) sublimation zone (on the vicinity of the pyrolysis zone). After the reaction, a dark central spot ca. 3 mm in diameter with a raised rim is seen to have formed on the surface of the target (hereafter referred to as the *crown*). The crown formation on the target is illustrated in the right panel of Fig. 1. In addition, some fine soot forms on the molybdenum target holder (hereafter referred to as *holder* material). The total mass of the powders collected from the crown and the holder was ca. 30–40 wt% of the starting mass of the anthracene. The rest of the sublimed anthracene and anthracene products were flushed away with the buffer gas. The as-produced material morphology was studied using scanning electron microscopy (SEM)—Leo 1530 and transmission electron microscopy (TEM)—Tecnai F30. X-ray diffraction (XRD) analysis was performed using a Siemens D500 analyser (Cu$K\alpha$ line). The products were also investigated via Fourier transform Raman spectroscopy (Bruker IFS 100 equipped with a 1064 nm excitation laser) and FT-IR absorption spectroscopy with a Bruker IFS113 Fourier transform spectrometer. To conduct optical absorption spectroscopy, the samples were prepared by thoroughly dispersing the product in acetone in an ultrasonic bath and then subsequently dropping the solution onto a heated KBr single crystal giving a thin homogeneous film.

3. Results

Fig. 2 shows typical SEM images of the products collected from the crown and holder. The crown products contain relatively large spherical objects (microspheres) with the diameters between 1 and 2 μm. A few graphite crystallites were also present (see arrow in Fig. 2A) and are remnants from the neutral graphite matrix that are picked up in the collection process of the crown material. Occasionally, smaller carbon nanoparticles with diameters below 200–300 nm were also found (marked by an arrow in Fig. 2B). The products formed on the holder (Fig. 2C) were more homogeneous (in size) and consisted *only* of CNS (100–400 nm in diameter). Further structural details were obtained from TEM investigations (Fig. 3). The initial TEM studies suggested both the crown and holder products consist entirely of solid carbon spheres. More detailed studies (discussed below) show some anthracene to be present in sample obtained from the holder. In addition, the TEM studies occasionally showed carbon-onion like structures to be present (arrowed in Fig. 3C). These structures can be considered as giant-fullerenes (nested carbon cages are clearly seen). The EDX studies (Fig. 3D) showed only carbon to be present (however, the possibility of some hydrogen being incorporated in the CNS cannot be excluded). There is also a very weak signal from oxygen that can probably be attributed to moisture contamination. The Au, Fe and Co signals in the spectrum arise from the TEM grid and grid holder. In Fig. 3E, an HRTEM image of CNS collected from the target holder is presented. In order to enhance the clarity of the HRTEM image, a skeletisation procedure has been applied. This numerical procedure is based on the digital filtering of user set gray level thresholds. The technique helps highlight the structural features of the CNS. The HRTEM images (e.g. Fig. 3E, F) point to the spheres being comprised of small curved aromatic graphene-like layers with lengths of a few nm. Some of these graphene units are parallelly stacked (in the 0 0 2 direction). Disordered atomic arrangement and disturbed lattice fringes are clearly seen. This is obviously a consequence of the amorphous structure of the CNS. The interspacing between the aromatic layers varies between 0.36 to 0.5 nm. The smaller value is typical for sp^2 hybridized carbon nanostructures and is a slightly higher interlayer distance than found in pyrolytic graphite. Unlike other carbon nanostructures (e.g. nanotubes), we found the CNS to remain stable under the TEM electron beam (300 kV), even after extended exposure periods. This suggests that the unclosed graphene layers (Fig. 3E)

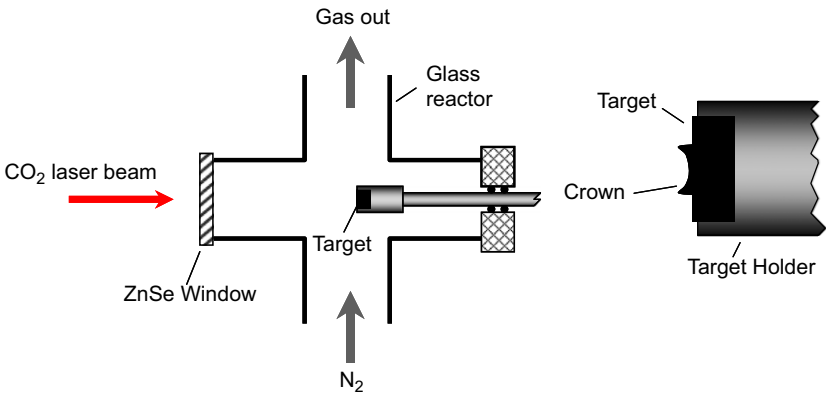

Fig. 1. Experimental set-up of the CO_2 laser-assisted pyrolysis reactor.

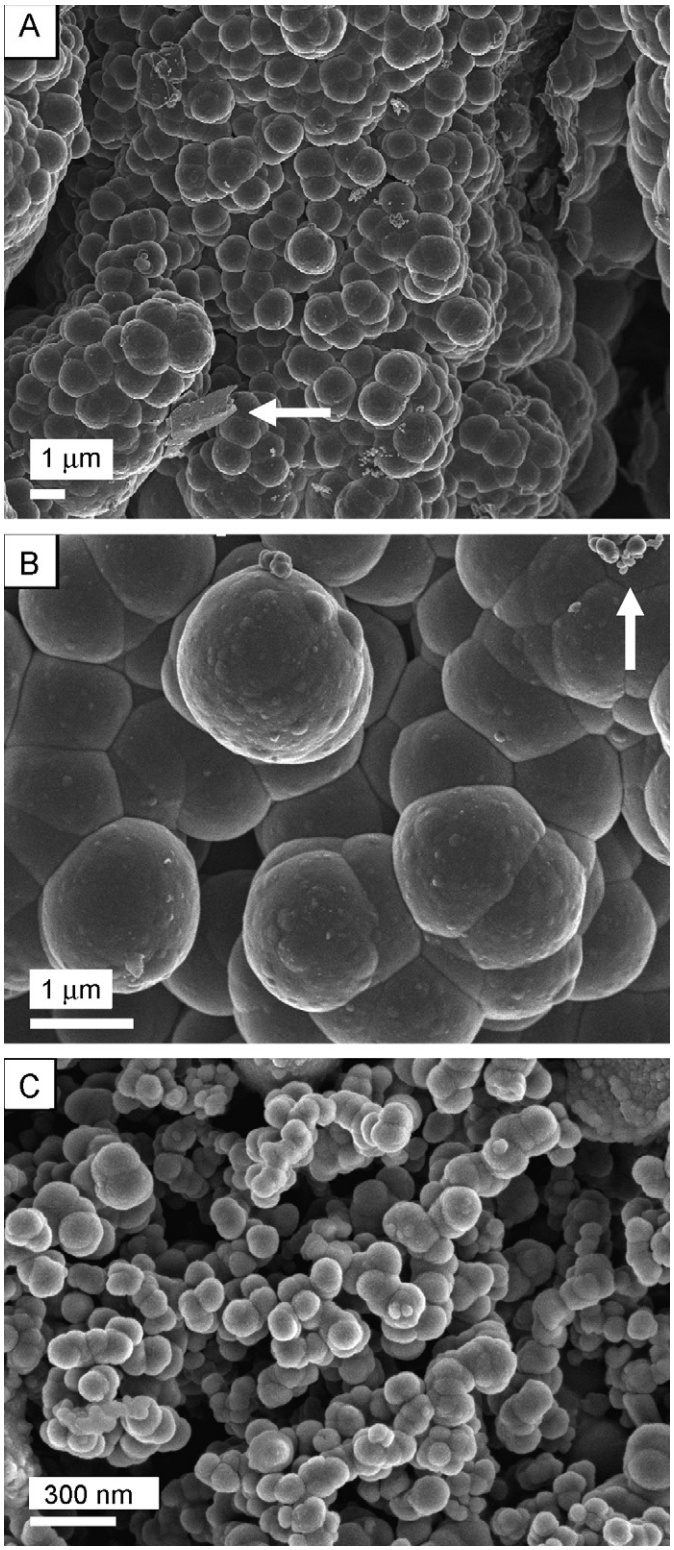

Fig. 2. SEM images of the products collected from the crown (A,B) and holder (C).

are bound to each other via strong (covalent) bonds, rather than weak van der Waals interactions.

Fig. 4A and C show the XRD diffraction patterns for both the crown and holder products, respectively. Material from the crown shows very strong diffraction peaks, which can be ascribed to graphite. This is due to graphite from the neutral graphite matrix (since the diffraction peaks of well-crystallized particles are much stronger and narrower than that of the nanocrystalline phase, the observed signal ratio in Fig. 4 does not provide any information on the carbon spheres content). No graphite peaks are observed for material from the holder, confirming the initial assertion that the graphite peak for material from the crown arises from the matrix graphite. Powder extracted from the holder, however, shows strong peaks related to undecomposed anthracene. The presence of only (0 0 l) anthracene diffraction peaks indicates that the crystallites are arranged in one crystallographic direction. This might be due to adsorption of anthracene on the CNS surface. Moreover, the possibility of non-covalent interactions between graphene layers and anthracene molecules emphasize this hypothesis. Previous studies have shown that anthracene adsorbs on carbon nanotube surfaces [34]. Further, the XRD patterns show a very broad peak around 25–26° for the products from both the crown and holder. This peak is associated with the ordering of graphene sheets in the 0 0 2 direction. Subtraction of the relatively intense and sharp graphite and anthracene responses (Fig. 4B and D) allows a more detailed analysis of the 0 0 2 diffraction peak. Analysis of both the position and shape of the 0 0 2 peak allows one to obtain average values for the interlayer distance (d_{002}), as well as for L_c in graphitic materials [34]. L_c is the average size of the graphene coherently diffracting domain (built from the parallel and flat aromatic layers) in the 0 0 2 direction. Here, L_c was estimated by applying the William–Hall formula [35]:

$$L_c = \frac{0.9\,\lambda}{\mathrm{FWHM}\cos\theta - 4\varepsilon\sin\theta}$$

where, FWHM is the full-width at half-maximum of the diffraction peak 0 0 2, λ is the wavelength of the X radiation, and ε is the lattice strain. The lattice strain was calculated by the formula $\varepsilon = |d - d_0/d_0|$, where d and d_0 stand for the interlayer distance (d_{002}) in the sample and graphite, respectively. The values of d_{002} were found to be 0.3561 and 0.3583 nm for the crown and holder products, respectively. These values are higher than the interlayer distance in HOPG pyrolotytic graphite (0.3354 nm). This increase of d_{002} (in comparison to well-crystallized graphite) suggests a high density of defects (vacancies, pentagons and heptagons incorporated in the lattice) in the carbon spheres. The calculated L_c values were 0.98 and 0.69 nm for the crown and holder products, respectively. On the basis of the d_{002} distance, one can estimate the average size of the graphene domain in the carbon spheres. The domains are built on 3 and 2 graphene layers for the crown and holder samples, respectively. Both, the higher d_{002} distances and very low L_c indicate low structural ordering in the obtained carbon spheres. This is in full agreement of the amorphous structure of the CNS observed in the TEM studies. It is worth noting that the crown products have a higher graphitization degree than those from the holder. The reaction temperatures at the crown are obviously higher than at the holder and a higher temperature might enable higher graphitization degrees. However, none of these materials can be considered as crystalline structures, per se.

Further details regarding the structure of the products were obtained by Raman spectroscopy (Fig. 5). The spectra were collected within the 1000 and 2000 cm^{-1} range, corresponding to the wavenumber range that provides the most valuable data on the structure of carbon materials. The spectra show two broad Raman bands at around 1300 and 1585 cm^{-1} [36]. The latter band corresponds to the E_{2g} mode (stretching vibrations) in the basal plane of the crystalline graphite (G graphitic peak). The width of the G band is related to the extent of disorder within the carbon sp^2 plane graphene layer. The band located at 1300 cm^{-1} (D band) is associated with disorder; this forbidden mode becomes active due to the lack of long-range order in amorphous and quasi-crystalline forms of carbon materials (symmetry breaking). The

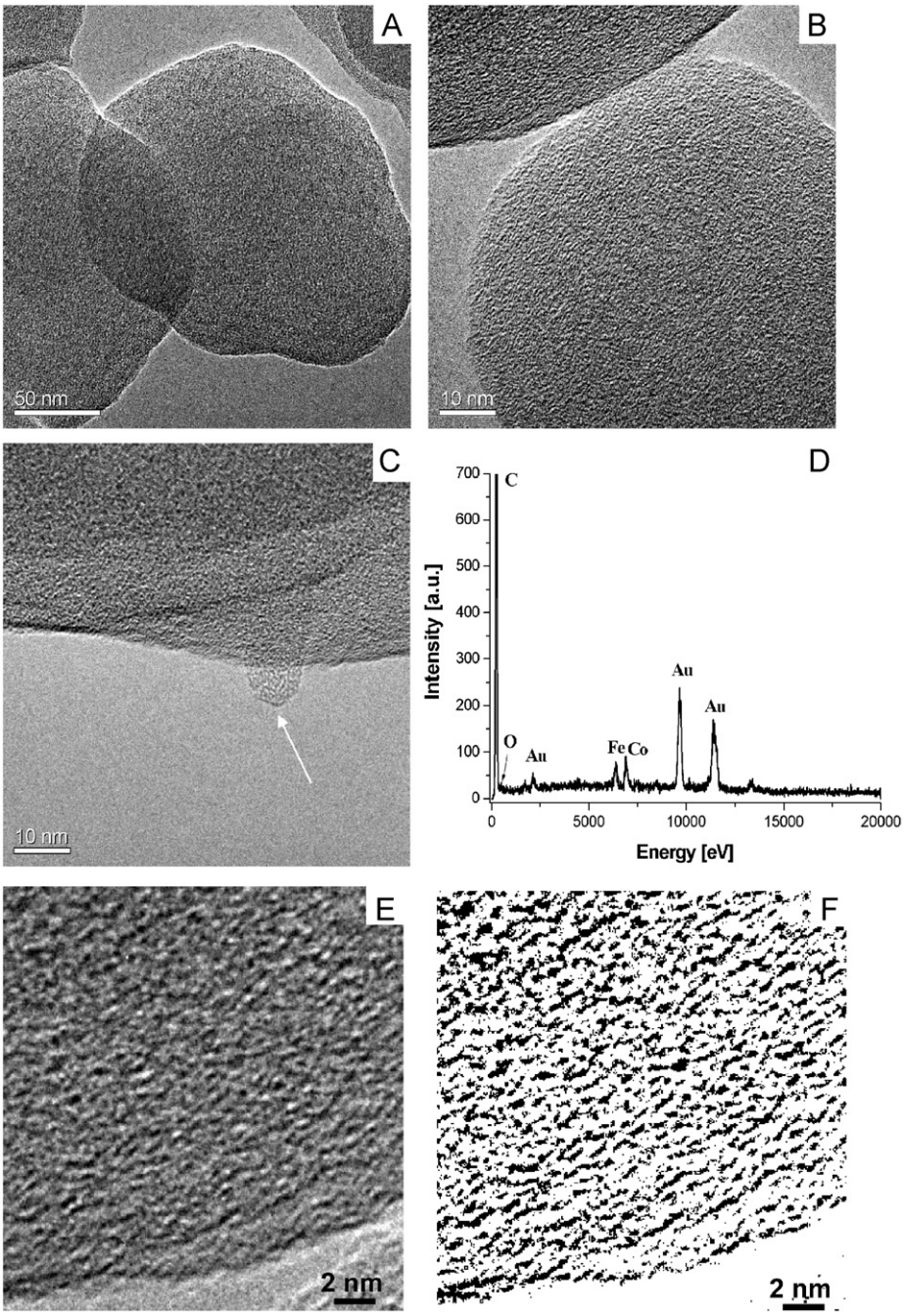

Fig. 3. TEM images of the products collected from holder (A–C), corresponding EDX spectrum (D) and HRTEM images (E, F).

intensity of the *D* band can also be enhanced by the presence of small graphitic domains (finite size effect), other imperfections such as substituted N or B atoms, sp^3 carbon, and the effects of finite particle size. Rather surprisingly the Raman spectrum does not contain any signals that can be ascribed to anthracene which the XRD data suggests should be present. Anthracene has a well-defined Raman response, with peaks appearing at 1010, 1163, 1185, 1260, 1403, 1480 and 1557 cm^{-1}. In this case the anthracene signals in Raman spectrum are not seen because they can overlap with very broad signals from CNS and so can be washed out. Finite size effects can also wash out anthracene signals. Further, the lack of an anthracene Raman response can also be due to anthracene adsorption on CNS surface as suggested above. Previous studies have shown that adsorption of polyaromatic hydrocarbons (including anthracene) on single-walled carbon nanotubes significantly alters their Raman response [37]. Further, these studies showed that the adsorption of anthracene on the single-walled carbon nanotubes increased the *D* band intensity and broaded the *G* band.

In order to improve the accuracy of spectroscopic parameter determinations, such as peak position, FWHM or band integral intensity, a curve deconvolution procedure was performed (Fig. 5). The *G* band is upshifted by 2–3 cm^{-1} in both samples as compared to that for HOPG (1582 cm^{-1}). This is a consequence of a decrease in the size of L_a (L_a is the diameter of the graphene basal plane) [38]. Tuinstra and Koenig's formula ($L_a = 4.35 \cdot I_G/I_D$, where I_G and I_D denote the integral intensities of the *G* and *D* bands, respectively) allows one to estimate L_a. However, in this case this equation cannot be applied because the correlation factor of 4.35 is valid only for a 488 nm excitation laser. It has been reported

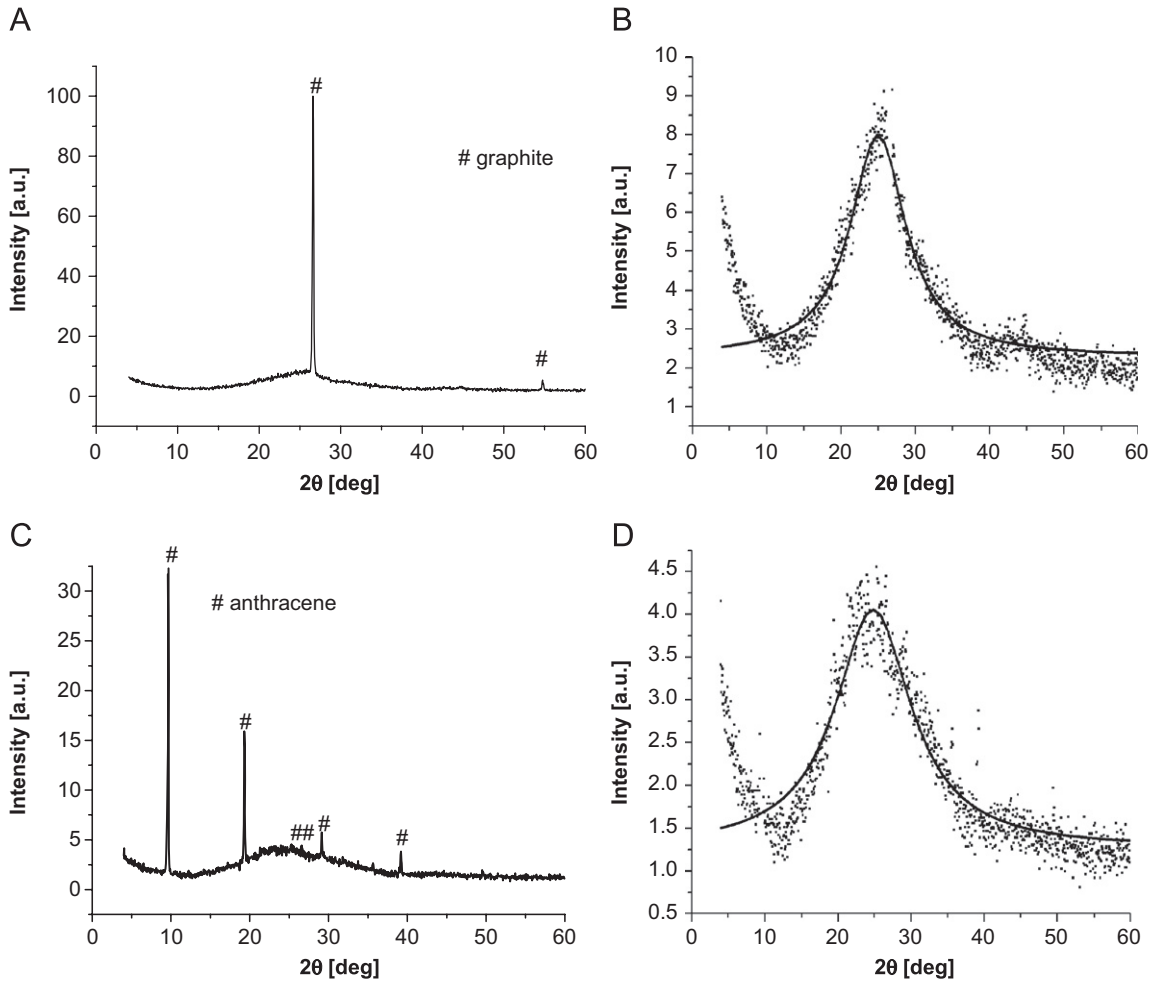

Fig. 4. XRD diffraction patterns of the products collected from the crown (A) and holder (C). Images (B) and (D) present the enlarged (002) diffraction peaks for crown and holder, respectively.

previously that the width of the *G* band is a convenient indicator of the L_a crystallite size [38]. In both cases (crown and holder samples) the width of the *G* band is between 80 and 90 cm^{-1}. These values point to an L_a size of between 2 and 3 nm. The elucidated L_a values correspond to the flat regions in the graphene layers in CNS. This is in good agreement with our HRTEM studies, which show that the size of the straight fringes do not exceed a few nanometers (e.g. Fig. 3E and F).

In order to further characterize the obtained products, FT-IR measurements were performed. Infrared spectroscopy is a technique highly suited to study the linking between aromatic graphene layers as well as moieties attached to the CNS surface. Fig. 6 shows the FT-IR spectra after strapping the background. The features localized below 1000 cm^{-1} in the crown and holder products can be attributed to vibrations from hexagonal graphene rings in the amorphous carbon lattice and C–H out of plane deformation. Ferrari et al. [39] found similar bands in the IR spectra of amorphous carbon nanoparticles. However, the vibrations of small moieties that link unclosed graphene layers (Fig. 3E,F) should be also considered in the analysis of the IR spectra. The peaks in the crown product located between 1000 and 1600 cm^{-1} can be ascribed to the following modes: C–C stretching and skeletal C=C streching. The peak at 1960 cm^{-1} can originate from the assymetric vibration of accumulated double bond system (C=C=CH_2). Moreover, the broad bands at 2600, 2860 and 2960 cm^{-1} can be assigned to C–H stretching vibrations. The variety of bands clearly indicates that hydrogen is bound to sp^3, sp^2 and aromatic carbon atoms. The IR spectrum from the holder sample contains fewer absorption peaks. This points to a simpler surface composition. The following bands are visible: 1223 and 1400 cm^{-1} (C–C stretching and skeletal C=C streching), 1728 cm^{-1} (C=O stretching mode). Broad bands at 2600 and 2800 cm^{-1} are also observable and are assigned to C–H stretching modes. The weak broad band at 3300 cm^{-1}, which appears in the spectra from both the crown and holder samples, is due to O–H stretching vibrations (probably moisture contamination via surface adsorption). Obviously, the contribution of anthracene cannot be overlooked in the spectrum of the holder product.

4. Discussion

The present work is the first report on the use of a low-power (30 W) CW CO_2 laser for synthesizing CNS via the direct decomposition of anthracene. In this study, the addition of graphite in the target matrix is required to improve the laser beam coupling to the target to enable the direct decomposition of the anthracene, viz, this laser power (30 W) is the lower limit for such a reaction. There are few reports on the use of CO_2 laser operating at higher power in the synthesis of carbon nanostructures. For example, Galvez et al. [33] investigated the synthesis of carbon nanoparticles by laser decomposition of gaseous

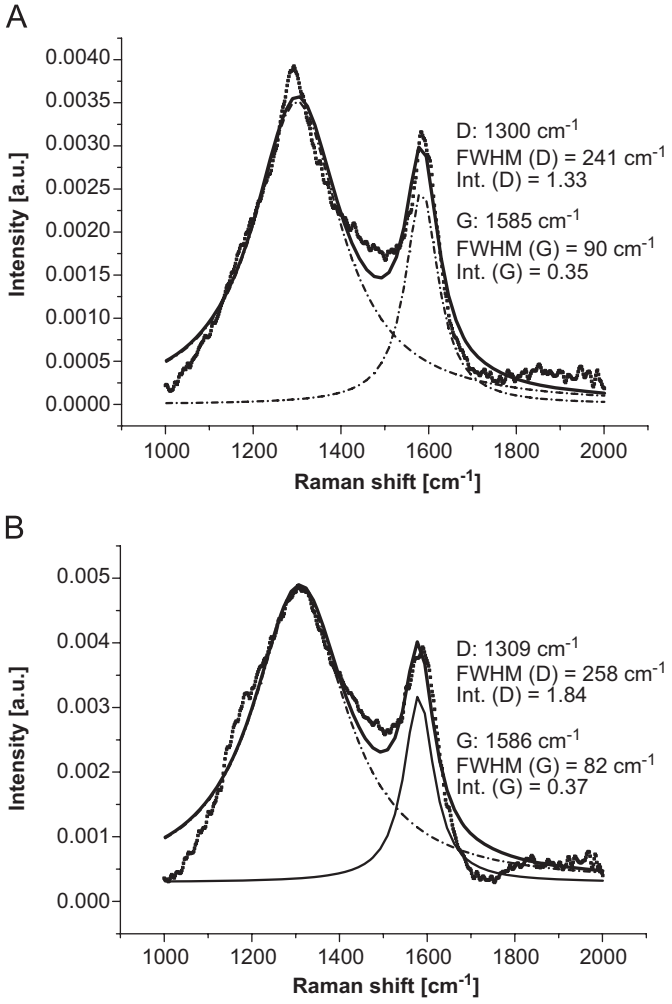

Fig. 5. Raman spectra of the products collected from the crown (A) and holder (B).

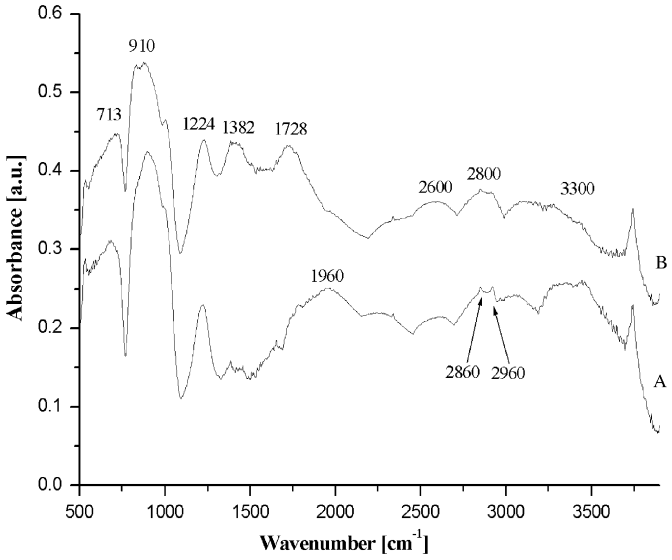

Fig. 6. FT-IR spectra of the products collected from the crown (A) and holder (B).

hydrocarbons as a function of power (ca. 300–800 W). The use of higher powers caused a temperature increase in the pyrolysis zone and enhanced the crystallinity of the as-formed carbon nanoparticles. Choi et al. [29] irradiated the acetylene flame by high power (up to 3000 W) and obtained well graphitized hollow carbon nanoparticles (50–100 nm in diameter). Unlike our work presented here where no gaseous feedstock is used, the above cited works, all used a flowing gaseous feedstock. Thus it is hard to directly compare our work with these. However, it is a reasonable assumption that the use of higher laser powers for anthracene pyrolysis would result in similar CNS but with higher graphitisation degrees.

In our system, the significant differences in temperature between where the laser couples to the target and outside this region on the target holder (cooler) are reflected in the morphology of the crown and holder products. At the center of the target where the laser couples (where the temperature is at its highest), simultaneous anthracene vaporization and decomposition occurs. The C–H bond (415 kJ/mol) is much weaker than the C–C bond energy in aromatic rings (602 kJ/mol) [40]. Hence, the laser irradiation preferentially breaks C–H bonds, leading to the creation of large radicals. The C–C aromatic bond, however, can also be broken and this leads to the formation of opened radicals. The laser irradiation and intercollision between radicals and excited molecules will create simple organic radicals: CH_3, C_2H_5, $H_2C{=}CH$ as well as H or H_2. These as-formed active species reduce their potential energy via collisions with other radicals and molecules. This will lead to aggregation such that bigger and bigger clusters form eventually yielding the observed CNS. The above considerations are consistent with previous theoretical and experimental studies [41,42]. They showed that fullerenes and fullerene-related particles are formed during collisions of polycyclic aromatic hydrocarbon (PAH) substructures with smaller and simpler hydrocarbons or radicals.

It is then worth asking, how are these small graphene layers linked in the volume of the carbon spheres? As discussed above, collisions of created radicals aggregate forming a bigger cluster. FT-IR spectra indicate a variety of C–C bonds in the investigated samples. Obviously, a fraction of them are localized on the carbon spheres surfaces (and saturates dangling bonds with hydrogen, C–H bands), however, the others will be incorporated within the structure. The broken lattice fringes (unclosed aromatic graphene-like layers) seen in the HRTEM images could be attributed to such bridging links. The crown and holder products are comprised of solid particles, which are insoluble in various solvents (acetone, hexane, toluene, etc.), even under sonication. This implies that the aromatic structure is not formed by aggregation caused by physical (non-covalent) interactions but that the aromatic graphene-like layers form a cross linked network in the obtained CNS.

The crown product exhibits a higher graphitization degree than those from the holder (L_c values are higher). This increase of crystallographic ordering for the crown microspheres results from their exposure to higher temperatures (the laser irradiation). Improved graphitization at higher temperatures is well documented for various nano-carbon materials [43–45].

The difference in the diameters of the two samples (crown and holder) arises due to the difference in concentration of available species (from the laser evaporation/decomposition). At the target surface where the crown forms these species are very dense and so agglomeration rates are relatively high leading to large microspheres, whereas the density of active species in the reaction chamber is reduced so that species that form in the chamber volume and then collect on the holder must invariably be smaller. A more homogeneous sample of smaller nanospheres condenses on the holder, which can be also attributed to cooler temperatures. The active transport of the carbon spheres from the irradiation zone to the holder is caused by two factors: (i) thermal diffusion and (ii) buffer gas flow. The presence of smaller spheres

in crown product (arrow in Fig. 2A) suggests some kind of backward flow rather than real cross-mixing of crown and holder products. This formation mechanism in which graphitic platelets add to the surface of a growing CNS can also explain why CNS can be larger than primary soot particles, which are always between 10 and 50 nm regardless of fuel type [46]. It has been suggested that primary soot particles grow from the center of the particle and this explains their limited diameter [47]. Further, primary soot particles are more fractal in nature [48] while CNS tend to be relatively more ordered in that they are composed of platelets.

As the formed CNS are transported from the irradiation zone to the holder they will also be in contact with the anthracene vapor (sublimed from cooler regions of the target). The sublimed anthracene can adsorb onto the CNS surface. This explains the presence of anthracene in the holder product and is further supported by the very recent reports in which various aromatic hydrocarbons (e.g. benzene [49], naphthalene [50]) are shown to adsorb on carbon materials directly from the gas phase.

Further, the dangling bonds on the surface and the edges of carbon spheres will be saturated with hydrogen or simple organic moieties (e.g. methyl or ethyl groups). The two peaks in the FT-IR spectra related to C–H stretching modes indicate that hydrogen saturate both aliphatic and aromatic surface carbon atoms. These surface features can act as linkers to functionalize CNS with other organic moieties in order to e.g. improve their dispersion stability in organic or polar solvents. This provides them with application potential for the synthesis of novel polymer-grafted carbon nanomaterials.

Further, the presented synthesis method for carbon micro- and nanospheres (from the crown and holder respectively) also contains traces of graphite and antrahcene that can easily be removed by facile purification procedures. Two simple routes to remove anthracene from the holder product can be followed: (i) dissolution by sonication or refluxing in a non-polar solvent (e.g., hexane, toluene) or (ii) thermal annealing at moderate temperatures (300–400 °C) [51]. Graphite from the crown sample can be removed via a one-step sedimentation assisted route in which the graphite particles sink while the carbon spheres remain suspended in solution [52].

5. Conclusions

To conclude, we have developed a fast and efficient technique to synthesize uniform CNS in bulk. The presented route does not require a supplementary catalyst or hydrocarbon feedstock. Moreover, a low-cost starting material (anthracene) was used. Temperature differences and differences in concentrations of the active species in the reaction chamber and at the target face lead two product morphologies with differing size distributions and crystallinity. Our detailed findings point to the CNS being comprised of small-unclosed aromatic graphene-like layers which are connected together with simple organic linkers. The results suggest that laser beam partially breaks C–H bonds in anthracene molecules, and as the created large radicals aggregate CNS are formed. It is likely that CNS can be also obtained from other solid aromatic hydrocarbons via this technique.

Acknowledgments

This work was supported by the Ministry of Science and Education through the Department of Chemistry, Warsaw University under Grant no. N204 096 31/2160. M.B. thanks the DFG (grant RU 1540/1-1) and the Foundation for Polish Science (FNP) for financial support. M.H.R. thanks the DFG for support via PI 440/4.

References

[1] H.W. Kroto, J.R. Health, S.C. O'Brien, R.F. Curl, R.E. Smalley, Nature 318 (1985) 162–163.
[2] S. Reich, C. Thomsen, J. Maultzsch, Carbon Nanotubes: Basic Concepts and Physical Properties, Wiley-VCH, New York, 2004.
[3] D. Ugarte, Nature 359 (1992) 707–709.
[4] D.C. Ruoff, V. Lorents, B. Chan, R. Malhotra, S. Subramoney, Science 259 (1993) 346–348.
[5] L. Xu, W. Zhang, Q. Yang, Y. Ding, W. Yu, Y. Qian, Carbon 43 (2005) 1090–1092.
[6] K. Niwase, T. Homae, K.G. Nakamura, K. Kondo, Chem. Phys. Lett. 362 (2002) 47–50.
[7] C. Wu, X. Zhu, C. OuYang, S. Hu, L. Lei, Y. Xie Y, Inorg. Chem. 45 (2006) 8543–8550.
[8] Y.Z. Jin, C. Gao, W.K. Hsu, Y. Zhu, A. Huczko, M. Bystrzejewski, M. Roe, C.Y. Lee, S. Acquah, H.W. Kroto, D.R.M. Walton, Carbon 43 (2005) 1944–1953.
[9] M. Zheng, J. Cao, X. Chang, J. Wang, J. Liu, X. Ma, Mater. Lett. 60 (2006) 2991–2993.
[10] Y.Z. Jin, C. Gao, H.W. Kroto, T. Maekawa, Mol. Rapid Commun. 26 (2005) 1133–1139.
[11] W. Li, D. Chen, Z. Li, Y. Shi, Y. Wan, J. Huang, J. Yang, D. Zhao, Z. Jiang, Electrochem. Commun. 9 (2007) 569–573.
[12] Y.Z. Jin, Y.J. Kim, C. Gao, Y.Q. Zhu, A. Huczko, M. Endo, H.W. Kroto, Carbon 44 (2006) 724–729.
[13] C. Wang, C. Xiangfeng, W. Mingmei, Sensor. Actuat. B 120 (2007) 508–513.
[14] C. Velasco-Santos, A.L. Martinez-Hernandez, V.M. Castano, J. Phys. Chem. B 108 (2004) 18866–18869.
[15] Z.X. Liu, J.N. Park, S.H.R. Abdi, S.K. Park, Y.K. Park, C.W. Lee, Top. Catal. 39 (2006) 221–226.
[16] J.Y. Miao, D.W. Hwang, K.V. Narasimhulu, P.I. Lin, Y.T. Chen, S.H. Lin, L.P. Hwang, Carbon 42 (2004) 813–822.
[17] J.Y. Miao, D.W. Hwang, C.C. Chang, S.H. Lin, K.V. Narasimhulu, L.P. Hwang, Diamond Relat. Mater. 12 (2003) 1368–1372.
[18] Y. Xia, Z. Yang, R. Mokaya, J. Phys. Chem. B 108 (2004) 19293–19298.
[19] X.B. Yan, T. Xu, S. Xu, G. Chen, H.W. Liu, S.R. Yang, Carbon 42 (2004) 2769–2771.
[20] J. Yao, H. Wang, J. Liu, K.Y. Chang, L. Zhang, N. Xu, Carbon 43 (2005) 1709–1715.
[21] J. Liu, M. Shao, Q. Tang, X. Chen, Z. Liu, Y. Qian, Carbon 41 (2002) 1682–1685.
[22] B. Liu, D. Jia, Q. Meng, J. Rao, Carbon 45 (2007) 668–670.
[23] Z. Lou, Q. Chen, J. Gao, Y. Zhang, Carbon 42 (2004) 219–232.
[24] Z. Wang, L. Yu, W. Zhang, Z. Zhu, G. He, Y. Chen, G. Hu, Phys. Lett. A 307 (2003) 249–252.
[25] I. Loa, C. Moschel, A. Reich, W. Assenmacher, K. Syassen, M. Jansen, Phys. Stat. Sol. B 223 (2001) 293–297.
[26] C. Kramberger, M. Loffler, M.H. Rummeli, A. Gruneis, R. Schonfelder, O. Jost, T. Gemming, T. Pichler, B. Buchner, Phys. Stat. Sol. B 243 (2006) 3050–3053.
[27] M.H. Rummeli, M. Loffler, C. Kramberger, F. Simon, F. Fulop, O. Jost, R. Schonfelder, A. Gruneis, T. Gemming, W. Pompe, B. Buchner, T. Pichler, J. Phys. Chem. C 111 (2007) 4094–4098.
[28] M.H. Rummeli, E. Borowiak-Palen, T. Gemming, T. Pichler, M. Knupfer, M. Kalbac, L. Dunsch, O. Jost, S.R.P. Silva, W. Pompe, B. Buchner, Nano Lett 5 (2005) 1209–1215.
[29] M. Choi, I.S. Altman, Y.J. Kim, P.V. Pikhitsa, S. Lee, G.S. Park, T. Jeong, J.B. Yoo, Adv. Mater. 16 (2004) 1721–1725.
[30] M.H. Rummeli, C. Kramberger, M. Loffler, M. Kalbac, H.W. Hubers, A. Gruneis, A. Barreiro, D. Grimm, P. Ayala, T. Gemming, F. Shaffel, L. Dunsh, B. Buchner, T. Pichler, Nanotechnol 17 (2006) 5469–5473.
[31] B. Oksengorn, C.R. Acad. Sci. Paris, Chimie 4 (2001) 873–878.
[32] V.Z. Mordkovich, Chem. Mater. 12 (2000) 2813–2818.
[33] A. Galvez, N. Helin-Boime, C. Reynaurd, C. Clinard, J.N. Rouzaud, Carbon 40 (2002) 2775–2789.
[34] J. Zhang, J.K. Lee, Y. Wu, R.W. Murray, Nano Lett 3 (2003) 403–407.
[35] H.G. Klug, L.E. Alexander, X-ray Diffractions Procedures for Polycrystalline and Amorphous Materials, Wiley, New York, 1971.
[36] A.C. Ferrari, J. Robertson, Phys. Rev. B 61 (2000) 14095–14107.
[37] T.G. Hedderman, S.M. Keogh, G. Chambers, H.J. Byrne, J. Phys. Chem. B 110 (2006) 3895–3901.
[38] F. Tuinistra, J.L. Koenig, J. Chem. Phys. 53 (1970) 1126–1130.
[39] A.C. Ferrari, S.E. Rodil, J. Robertson, Phys. Rev. B 67 (2003) 155306–155319.
[40] R.C. Merkle, R.A. Freitas, J. Nanosci. Nanotechnol. 3 (2003) 319–324.
[41] A. Violi, V. Venkatnathan, J. Chem. Phys. 125 (2006) 54302.
[42] A. Goel, P. Hebgen, J.B. Vander Sande, J.B. Howard, Carbon 40 (2002) 177–182.
[43] V.A. Davydov, A.V. Rakhmanina, J.P. Boudou, A. Thorel, H. Allouchi, V. Agafonov, Carbon 44 (2006) 2015–2020.
[44] M.A. Wilson, A. Moy, H. Rose, G.S.K. Kannangara, B.R. Young, D.G. McCulloch, D.J.H. Cockayne, Fuel 79 (2000) 47–56.
[45] M. Bystrzejewski, H. Lange, A. Huczko, Fuller. Nanotub. Car. N. 15 (2007) 167–180.
[46] M.H. Rummeli, C. Kramberger, A. Gruneis, P. Ayala, T. Gemming, B. Buchner, T. Pichler, Chem. Mater. 19 (2007) 4105–4107.

[47] K. Saito, A.S. Gordon, F.A. Williams, W.F. Stickle, Combust. Sci. Technol. 80 (1991) 103–112.
[48] M.M. Maricq, J. Aerosol Sci. 38 (2007) 141–156.
[49] M.R. Cuervo, E. Asedegbega-Nieto, E. Diaz, A. Vega, S. Ordonez, E. Castillejos-Lopez, J. Rodriguez-Ramos, J. Chromatogr. A 1188 (2008) 264–273.
[50] K. Inoue, K. Kawamoto, Chemosphere 70 (2008) 349–357.
[51] C.O. Ania, B. Cabal, C. Pevida, A. Arenillas, J.B. Parra, F. Rubiera, J.J. Pis, Water Res 41 (2007) 333–340.
[52] M. Bystrzejewski, A. Huczko, H. Lange, Mater. Chem. Phys. 107 (2008) 322–327.